Ab initio and quasiclassical trajectory study of the $N(^2D)+NO(X^2\Pi) \rightarrow O(^1D)+N_2(X^1\Sigma_g^+)$ reaction on the lowest $^1A'$ potential energy surface

Miguel González,[a] R. Valero, and R. Sayós[b]
Department de Química Física i Centre de Recerca en Química Teòrica, Universitat de Barcelona, C/Martí i Franquès 1, 08028 Barcelona, Spain

(Received 7 August 2000; accepted 28 September 2000)

In this work we have carried out *ab initio* electronic structure calculations, CASSCF/CASPT2 with the Pople's 6-311G(2d) basis set on the ground singlet potential energy surface ($1\,^1A'$ PES) involved in the title reaction. Transition states, minima and one $1\,^1A'/2\,^1A'$ surface crossing have been characterized, obtaining three NNO isomers with the energy ordering: NNO ($^1\Sigma^+$) $<$cyclic$-C_{2v}$ NON($^1A_1$)$<$NON($^1\Sigma_g^+$). Approximately 1250 *ab initio* points have been used to derive an analytical PES which fits most of the stationary points, with a global root-mean-square deviation of 1.12 kcal/mol. A quasiclassical trajectory study at several temperatures (300–1500 K) was performed to determine thermal rate constants, vibrational and rovibrational distributions and angular distributions. The dynamics of this barrierless reaction presents a predominant reaction pathway (96% at 300 K) with very short-lived collision complexes around the NNO minimum, which originate backward scattering and a similar fraction of vibrational and translational energy distributed into products. At higher temperatures other reaction pathways involving NON structures become increasingly important as well as the N-exchange reaction (3.02% of the branching ratio at 1500 K), this latter in accord with experimental data. It is concluded that the physical electronic quenching of $N(^2D)$ by NO should be negligible against all possible $N(^2D)+NO$ reaction channels.
© *2000 American Institute of Physics.* [S0021-9606(00)30448-2]

I. INTRODUCTION

The nitrous oxide molecule plays an important role in both combustion and atmospheric processes, participating also in the stratospheric ozone cycle. Among the main three processes of dissociation of this molecule,

$$N_2O(X\,^1\Sigma^+) \rightarrow O(^1D)+N_2(X\,^1\Sigma_g^+), \quad \Delta_r H^0_{0\ K}=83.92\ \text{kcal mol}^{-1}, \tag{1}$$

$$\rightarrow N(^2D)+NO(X\,^2\Pi), \quad \Delta_r H^0_{0\ K}=168.52\ \text{kcal mol}^{-1}, \tag{2}$$

$$\rightarrow O(^3P)+N_2(X\,^1\Sigma_g^+), \quad \Delta_r H^0_{0\ K}=38.55\ \text{kcal mol}^{-1}, \tag{3}$$

the first one constitutes an additional source of the highly reactive first excited electronic state of the oxygen atom produced by photodecomposition at heights above 25 km and for wavelengths below 220 nm in the stratosphere.[1] (The gas phase standard reaction enthalpies at 0 K for all reactions were derived from the experimental data of Ref. 2.) The main source of this electronic state is the ozone photodissociation in the 200–300 nm wavelength region. The first photodissociation process (1) has been used at the laboratory as a standard source of $O(^1D)$ atoms for the study of several bimolecular reactions.[3–5] The dissociation of the N_2O molecule in its ground electronic state can also take place through the spin conserving channel (2) or can predissociate through the spin forbidden process (3). Regarding the corresponding bimolecular processes, abundant theoretical[6,7] and experimental[8,9] data are available on the electronic quenching of $O(^1D)$ by N_2,

$$O(^1D)+N_2(X\,^1\Sigma_g^+)\rightarrow O(^3P)+N_2(X\,^1\Sigma_g^+), \quad \Delta_r H^0_{0\ K}=-45.37\ \text{kcal mol}^{-1}, \tag{4}$$

and about the reaction

$$O(^3P)+N_2(X\,^1\Sigma_g^+)\rightarrow N(^4S)+NO(X\,^2\Pi), \quad \Delta_r H^0_{0\ K}=75.01\ \text{kcal mol}^{-1}, \tag{5}$$

and also on its reverse reaction.[10,11] However, theoretical studies of the $N(^2D)+NO(X\,^2\Pi)$ reactions are nonexistent to our knowledge; only several experimental kinetic studies are available dealing with the thermal rate constant for the total removal of $N(^2D)$ by NO at 300 K, whose value ranges from $(3.5\pm0.3)\times10^{-11}$[12] to $(8.3\pm0.3)\times10^{-11}$ $\text{cm}^3\ \text{molecule}^{-1}\,\text{s}^{-1}$.[13]

There are several processes energetically accessible at room temperature for a $N(^2D)+NO(X\,^2\Pi)$ collision process:

[a]Electronic mail: miguel@qf.ub.es
[b]Electronic mail: r.sayos@qf.ub.es

 © 2000 American Institute of Physics

$$N(^2D)+NO(X\,^2\Pi)$$

$$\rightarrow N(^2D)+N'O(X\,^2\Pi), \quad \Delta_r H^0_{0\ K}=0\ \text{kcal mol}^{-1}, \tag{6}$$

$$\rightarrow O(^1S)+N_2(X\,^1\Sigma_g^+), \quad \Delta_r H^0_{0\ K}=-33.35\ \text{kcal mol}^{-1}, \tag{7}$$

$$\rightarrow O(^1D)+N_2(X\,^1\Sigma_g^+), \quad \Delta_r H^0_{0\ K}=-84.60\ \text{kcal mol}^{-1}, \tag{8}$$

$$\rightarrow O(^3P)+N_2(X\,^1\Sigma_g^+), \quad \Delta_r H^0_{0\ K}=-129.97\ \text{kcal mol}^{-1}, \tag{9}$$

$$\rightarrow N(^4S)+NO(X\,^2\Pi), \quad \Delta_r H^0_{0\ K}=-54.96\ \text{kcal mol}^{-1}. \tag{10}$$

The first one (6) includes both the inelastic/elastic processes (6a) and the N-exchange reaction (6b). The processes (7), (8) and (9) correspond to the reaction of formation of a N_2 molecule along with the atomic oxygen in a fundamental or excited state. From the total of 20 potential energy surfaces (PESs) which adiabatically correlate with reactants in C_s symmetry [i.e., $5(^1A')$, $5(^1A'')$, $5(^3A')$ and $5(^3A'')$],[14,15] only one (i.e., $^1A'$), 5 [i.e., $3(^1A')$ and $2(^1A'')$] and one (i.e., $^3A''$) PESs correlate with products for reactions (7), (8) and (9), respectively. Moreover, the lowest $^1A'$ PES also correlates with a ground state N_2O ($X\,^1\Sigma^+$) molecule. The physical electronic quenching process (10) implies at least nonadiabatic transitions between states of different multiplicity (e.g., $^1A'\rightarrow{}^3A'$ or $^1A'\rightarrow{}^5A'$), which may only take place if spin– orbit coupling interaction occurs. In spite of the large number of possible processes, the high efficiency observed for the removal of this excited nitrogen atom [i.e., a $N(^2D)$ atom is removed every two to three collisions with NO] provides strong evidence for reaction rather than physical quenching.[15] Furthermore, the existence of five adiabatic PESs involved in reaction (8) suggests that this exothermic reaction should furnish an important amount to the $N(^2D)$ total removal rate constant.

There is no theoretical information about all the regions of the lowest $^1A'$ PES, which would be necessary in a first approximation to the study of reaction (8). Nevertheless, the NNO molecule has been extensively studied both experimentally and theoretically, this information also being of relevance for the reaction of concern. The experimental vibrational energy levels up to 8000 cm^{-1} were measured in 1950 by Herzberg and Herzberg.[16] The vibrational spectrum below 8200 cm^{-1} was later studied by means of Fourier transform spectrometry[17,18] and more recently vibrational bands in the visible and near infrared were determined between 6500 and 11000 cm^{-1} by this same technique and between 11700 and 15000 cm^{-1} by intracavity absorption spectroscopy.[19] Studies of vibrational and rotational bands including isotopic substitution in more limited regions of the spectrum are reported by several authors.[20–22] This wealth of data has made feasible the construction of model force fields to provide potential surfaces for the N_2O molecule. Thus, the first quartic force field was derived employing standard perturbation theory.[23] Sextic force fields determined by several authors with a variety of methods also exist.[24–27] Other studies have been based on the construction of effective rovibrational Hamiltonians to account for the resonant interactions in the molecule.[28]

Referring to the theoretical studies, there are reports in the literature of several *ab initio* force fields for the N_2O molecule. In particular, quartic force fields at the SCF and CISD levels of theory[29] and at the CCSD(T) level[30] have been reported. The influence of the reference structure on the accuracy of the force field has been systematically explored at the SCF, CCD, and CCSD(T) levels, thus deriving also quartic force fields.[31] More recently, SCF and CCSD(T) sextic force fields have also been determined.[32,33] Studies of potential energy surfaces covering more extensive regions of the configuration space and excited electronic states also exist.[34–39] Peyerimhoff and Buenker performed an analysis of several electronic states characterizing also a linear NON ($^1\Sigma_g^+$) minimum in the ground PES.[34] This minimum has also been located more recently.[35–37] A cyclic NON C_{2v}-symmetric minimum has also been located on the ground PES of the system.[35–38] It is suggested to be an intermediate in the decomposition of the $O(N_3)_2$[36] and N_4O[39,40] azides, in which the final product is linear N_2O ($X\,^1\Sigma^+$). The more comprehensive analysis of the system to date was performed at a MCSCF level by Hopper[14] including about 30 N_2O electronic states, locating also the cyclic C_{2v}-symmetric ($^1A_1$) minimum. Potential surfaces aimed at the study of the photodissociation of the molecule through reaction (1) and its predissociation through reaction (3) have been constructed[9,41–43] covering only that portion of the surfaces connecting with these dissociation channels.

Our goal in the present study is to provide an accurate PES for the study of the reaction of electronically excited nitrogen atom $N(^2D)$ with the NO molecule [i.e., reaction (8)] through the lowest $^1A'$ PES which correlates with the N_2O molecule. It is thought that this reaction channel could account for an important part of the reactivity of the system.

In Sec. I a presentation of the *ab initio* methodology employed as well as of the stationary points obtained on the PES $^1A'$ is given. In Sec. II we provide a description of the analytical fit of the *ab initio* information and a detailed characterization of the PES obtained. In Sec. III we present a preliminary quasiclassical trajectory study (QCT) on the kinetics and dynamics of this reaction at 300 K and also at other higher temperatures. Finally, in Sec. IV we summarize the concluding remarks.

II. *AB INITIO* STUDY OF THE GROUND SINGLET PES

A. Computational procedure

The calculations presented in this work have been performed with the GAUSSIAN 98[44] and MOLCAS 4.1[45] packages of electronic structure calculations. The complete active space self-consistent field method (CASSCF)[46,47] was employed throughout this study, always choosing the lowest singlet root in C_s symmetry, which correlates with the $X\,^1\Sigma^+$ electronic state of the N_2O molecule (linear in its equilibrium geometry) and more generally with the $1\,^1A'$ electronic state (in bent geometries). The location of the stationary point geometries on the ground $^1A'$ PES was achieved by optimi-

TABLE I. Exoergicity and properties of reactants and products.[a]

	D_e (kcal/mol)	R_e (Å)	ω_e[b] (cm^{-1})	$\omega_e x_e$ (cm^{-1})	α_e (cm^{-1})	B_e (cm^{-1})	$\overline{D_e}$ (cm^{-1})
NO($X\,^2\Pi$)							
CASSCF/6-311G(2d)	128.23	1.1609	1878.0	16.252	1.82×10^{-2}	1.6753	5.35×10^{-6}
CASPT2/6-311G(2d)	140.73	1.1598	1857.9	13.303	1.71×10^{-2}	1.6785	5.48×10^{-6}
Experimental[c]	152.53	1.1508	1904.2	14.075	1.71×10^{-2}	1.6720	5.47×10^{-6}
$N_2(X\,^1\Sigma_g^+)$							
CASSCF/6-311G(2d)	210.36	1.1056	2334.6	13.674	1.65×10^{-2}	1.9697	5.61×10^{-6}
CASPT2/6-311G(2d)	212.55	1.1034	2316.7	14.075	1.73×10^{-2}	1.9776	5.76×10^{-6}
Experimental[c]	228.41	1.0977	2358.6	14.324	1.73×10^{-2}	1.9982	5.76×10^{-6}

	$E(N(^4S)\rightarrow N(^2D))$ (kcal/mol)	$E(O(^3P)\rightarrow O(^1D))$ (kcal/mol)	ΔD_e	(kcal/mol)[d]	ΔD_0
CASSCF/6-311G(2d)	66.00	51.51	−96.61		−95.96
CASPT2/6-311G(2d)	62.07	48.65	−85.24		−84.58
Experimental[c]	54.96	45.37	−85.48		−84.83

[a]Active spaces in *ab initio* calculations: CAS(11,8) and CAS(10,8) for NO and N_2, respectively.
[b]Masses of the most abundant isotopes are used: ^{14}N and ^{16}O.
[c]References 53 and 54. Spectroscopic constants for NO($X\,^2\Pi_{1/2}$).
[d]Exoergicity of reaction (8) with (AD_0) and without (ΔD_e) zero-point energy corrections (i.e., including ω_e and $\omega_e x_e$). The lowest spin–orbit states [i.e., NO($X\,^2\Pi_{1/2}$),N($^2D_{5/2}$) and O($^3P_2$)] were used for the experimental energies.

zation searches of both minima (MINs) and transition states (TSs) employing analytic gradients. Full characterization of them was performed by calculating the numerical Hessian matrix at the optimal geometries. Calculations at the second-order of perturbation theory based on a zeroth-order CASSCF wave function (CASPT2 method) using the G2 variant as implemented in MOLCAS 4.1[48] were applied to refine the stationary points obtained at the CASSCF level and to generate grids of points covering all the relevant portions of the PES. Altogether about 1129 points were calculated in this way, distributed in 822 points for the NNO nuclear arrangement and 307 for the NON one (see below). Although most of them are concentrated near the stationary points, the asymptotes have also been widely explored to provide a good description of the PES around the minimum energy path (MEP).

The full-valence active space of the NNO system has been used throughout this study, i.e., all the atomic $2s$ and $2p$ electrons are distributed among the corresponding derived bonding and antibonding MOs. This complete active space (CAS), comprising 16 electrons in 12 orbitals [CAS(16,12)], generates 35793 configuration state functions (CSFs) for the $1\,^1A'$ electronic state. The CASPT2 calculations based on this CASSCF wave function have been performed keeping the three atomic $1s$ core orbitals frozen. The standard Cartesian 6-311G(2d) basis set of Pople and co-workers[49,50] comprising 25 basis functions per atom has been employed in all the calculations. This basis set was obtained from the extensible computational chemistry environment basis set database, version 1.0, as developed and distributed by the Molecular Science Computing Facility.[51] Recent calculations on the ground and the first excited electronic states of the *cis*- and *trans*-NO dimers have shown that this basis set and method are accurately enough to furnish an accurate description on even more complex systems as compared with experimental data and larger calculations.[52]

B. Stationary points

The *ab initio* results obtained for reactants and products and the exoergicity of reaction (8) are presented in Table I. The geometries of the diatomic N_2 and NO molecules were fully optimized at both CASSCF and CASPT2 levels. Spectroscopic constants (i.e., $\omega_e, \omega_e x_e, \alpha_e, B_e, \overline{D_e}$) were derived from an analytical fit of a grid of *ab initio* points (i.e., 65 for N_2 and 62 for NO) using an extended-Rydberg functional form:

$$V(R) = -D_e\left(1+\sum_{i=1}^{n=5} a_i(R-R_e)^i\right)e^{-a_1(R-R_e)}, \qquad (11)$$

where R_e and D_e are the equilibrium bond length and dissociation energy of each diatomic molecule, respectively, and a_i are adjustable parameters. It is remarkable that the increase in accuracy of the dissociation energy of the diatomics as well as their equilibrium geometries when the correlation energy is added. The tendency is not so clear when considering the harmonic frequencies, which are closer to experiment at the CASSCF level, although the agreement is rather good in both cases. In spite of the overestimate of the atomic excitation energies and the underestimate of the dissociation energies, most important in the construction of an analytical PES to be used for kinetics and dynamics studies is the very good prediction of the exoergicity of reaction, whose value lies within 0.25 kcal mol^{-1} of the experimental value, probably because of a compensation of errors.

The geometries, frequencies and energies relative to reactants, $N(^2D)+NO(X\,^2\Pi)$, for all the stationary points characterized at the CASSCF level, as well as the CASPT2 results derived from local fits to grids of points calculated around the CASSCF structures are given in Table II. The local fits were performed by means of the SURVIBTM code of molecular rovibrational analysis[55] with the exception of the N_2O molecule (see below). A symmetry adapted internal co-

TABLE II. *Ab initio* CASSCF(16,12) and CASPT2(16,12)/6-311G(2d) properties[a] of the stationary points on the ground $^1A'$ PES.

Symmetry/ stationary point	Energy (kcal/mol)	$R_{e\,(NN)}$ (Å)	$R_{e\,(NO)}$[b] (Å)	α[c] (°)	ω_i[d] (cm^{-1})		
			$C_{\infty v}$				
MIN 2 (NNO)	−163.57	1.1343	1.1931	180.0	2256.9	1280.7	596.1
	−170.10	1.1355	1.1947	180.0	2223.7	1269.6	589.5
TS2	−95.48	1.1046	2.1331	180.0	2337.7	226.7i	119.5
	−88.20						
			$C_{2v}, D_{\infty h}$				
MIN 5	−50.83	2.4076	1.2038	180.0	1730.8	1107.0	463.3
	−62.71	2.4256	1.2128	180.0	1695.7	1056.4	434.4
MIN 6	−33.44	1.8346	1.3349	86.8	1132.4	426.2	968.3
	−46.72	1.7416	1.3547	80.0	1104.8	187.0	890.8
MIN 7	−96.04	1.1891	1.5651	44.7	1769.9	706.2	271.9
	−103.45	1.2054	1.5487	45.3	1731.0	757.2	303.2
MIN 8	−96.23						
	−85.89	1.1061	2.9785	21.4	2010.3	46.0	299.4
TS 5	−23.52	2.2915	1.3215	120.2	956.9	627.1i	1145.6
	−38.79	2.2650	1.3205	118.1	973.8	570.2i	1117.8
TS 6	−32.71	1.7112	1.3622	77.8	1110.0	624.4i	900.1
	−46.59	1.7950	1.3465	83.6	1117.5	302.7i	939.9
TS 7	−85.40	1.1228	1.9719	33.1	2137.2	462.8i	279.7
	−83.05	1.1176	2.1043	30.8	2025.9	336.8i	286.8
			C_s				
MIN 1	−0.37						
	−1.73	3.2166	1.1597	93.4	1801.7	43.9	12.3
MIN 3	−97.02	1.1054	3.1400	168.8	2336.4	38.3	25.8
	−86.10						
MIN 4	−0.13	4.2600	3.3370, 1.1606	137.0	1878.9	40.8	32.9
	−1.58	3.3416	2.6062, 1.1573	120.2	1854.3	141.6	78.8
TS 4	6.02	3.0199	2.0092, 1.1609	143.2	1804.4	145.4	446.8i
	1.90	3.0965	2.0914, 1.1571	140.8	1825.6	195.7	509.6i
TS 9	−85.45	1.1283	1.6025	101.3	1955.2	99.8	741.4i
	−88.65	1.1452	1.4122	101.4	1856.1	549.9	541.7i

[a]Energies are given relative to reactants [i.e., $N(^2D)+NO$]. The first number in each row corresponds to the CASSCF property and the second one to the CASPT2 value. In some cases the stationary points were found only at one level (CASSCF or CASPT2), in which case the energy is reported for the another level at the same geometry. Reactants and products absolute energies are equal to −183.690787 and −184.044083 H, respectively.

[b]Both NO distances are reported for NON (C_s) structures.

[c]α is the ∠NON angle for C_{2v}, $D_{\infty h}$ and NON (C_s) structures, or ∠NNO otherwise.

[d]Masses of the most abundant isotopes are used: ^{14}N and ^{16}O. The order of the harmonic frequencies for normal modes is as follows: Σ^+, Σ^+, $\Pi(C_{\infty v})$; Σ_u^+, Σ_g^+, $\Pi_u(D_{\infty h})$; A', A', $A'(C_s)$ and A_1, A_1, $B_1(C_{2v})$. Frequencies for equal symmetry modes are shown in decreasing order with the imaginary one at the end.

ordinates expansion in the bond lengths [Simons–Parr–Finlan (SPF),[56,57] with $R_{SPF}=(R-R_e)/R$] and a Taylor expansion in the bond angles were used with several degrees of the polynomial, seeking convergence in geometry, energy and harmonic frequencies. A reexpansion of the potential energy in a Taylor series of the normal mode vectors around the located stationary point was performed, using standard perturbation theory to determine the spectroscopic constants. The maximum estimated errors of these fits in geometry were about 0.03 Å for the bond lengths, though in most cases this errors were lower (~0.001 Å), and 2° for the bending angles, being in most cases lower than 0.1°. For the absolute energies a typical error of 10^{-3}–10^{-4} kcal/mol was committed, while the frequencies were subject to an uncertainty lower than 1% in most cases and reaching 6–25% in the worst cases. In Fig. 1 the CASPT2 structures and their relative energies within the ground $^1A'$ PES are displayed. In this figure, several reactive mechanisms can be distinguished. In the first one, the reacting $N(^2D)$ atom can attack the N end of the NO molecule with the system evolving through the deep NNO well and yielding products without another stable intermediate structures (route 1). An inspection of the CASPT2 points generated in the asymptotes revealed that no barrier seems to exist neither in the entrance channel nor in the exit channel leading to products. In a second path, the $N(^2D)$ atom would attack the O end of the NO molecule generating structures with the NON connectivity. In this case, in the entrance channel a van der Waals bent minimum (MIN 4) precedes a transition state (TS 4) with a barrier with respect to reactants of about 1.90 kcal/mol, connecting with a linear $D_{\infty h}$ minimum (MIN 5). From this minimum the oxygen atom can depart keeping C_{2v} symmetry through a series of minima (i.e., MIN 6, MIN 7 and MIN 8) and transition states (i.e., TS 5, TS 6 and TS 7) until it dissociates to products, $O(^1D)+N_2$ (route 2). The link between these two paths is TS 9, that is basically a stretched NNO structure which is near an intersection of the two lowest $^1A'$ PESs (see below); a third path would involve an interchange between these routes through TS 9, beginning in

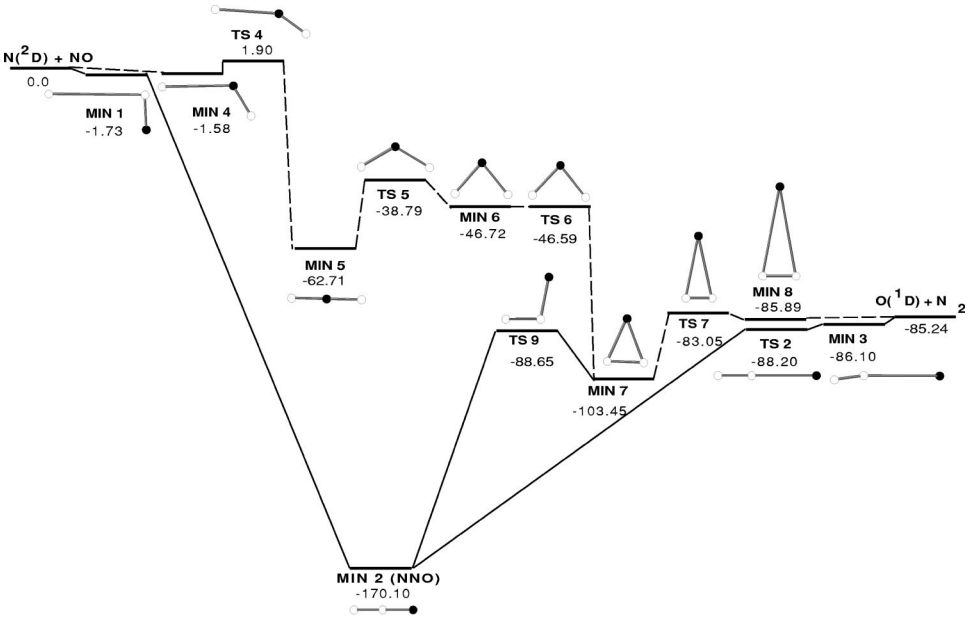

FIG. 1. Energy diagram at the CASPT2(16, 12)/6-311G(2d) level of the stationary points located on the ground $^1A'$ PES. Energies are given relative to reactants, $N(^2D)+NO$ in kcal/mol.

one route and finishing in the other one to produce finally $O(^1D)+N_2$ (route 3).

The electronic configuration for the ground state NNO molecule can be described as $(1-6\sigma)^2(1\pi)^4(7\sigma)^2(2\pi)^4$ in $C_{\infty v}$ symmetry. All the minima in the intermediate zone of the ground $^1A'$ PES (NNO, MIN 5, MIN 6 and MIN 7) present closed shell configurations that change into one another through the corresponding TSs. The stationary points placed in the entrance and exit zones show a mixing of different reactant and product-like open shell configurations, which transform gradually into the former closed shell configurations as the bond lengths shorten. The TS 9 linking routes 1 and 2 is a particular case because of its proximity to the excited $2\,^1A'$ PES, in which a single excitation to the first virtual a' molecular orbital has taken place. Thus, a certain amount of this excited configuration is found in TS 9.

In Table III a survey of the best experimental and previous *ab initio* geometries and harmonic frequencies of the NNO molecule is given and compared with the present calculations. In order to obtain a good estimate of the N_2O properties, a dense grid of about 185 *ab initio* CASPT2 points distributed around the N_2O optimal CASSCF structure were fitted to an analytical expression different to that employed for the rest of points (see below). CASPT2 frequen-

TABLE III. *Ab initio* and experimental data about the $NNO(X\,^1\Sigma^+)$ molecule.

Ab initio	D_e (kcal/mol)[a]		D_0 (kcal/mol)		$R_{e\,(NN)}$ (Å)	$R_{e\,(NO)}$ (Å)	ω_i[b] (cm^{-1})		
MCSCF-CI/DZ+d[c]	71.95	-	-	-	1.144	1.252	-	-	-
CCSD(T)/ ANO[5s4p2d1f][d]	-	-	-	-	1.1311	1.1874	2285.9	1299.1	604.3
MCQDPT(16,12)/ TZDP[e]	79.7	-	77.4	-	1.13	1.21	2340	1302	510[i]
BD(T)/cc-pVTZ[f]	-	-	-	-	1.132	1.189	2286	1299	604
CASPT2(16,12)/ 6-311G(2d) (this work)	84.85	170.10	81.39	165.98	1.1355	1.1947	2223.7	1269.6	589.5
				Experimental					
IR data[g]	-	-	-	-	1.1273	1.1851	2282.1	1298.3	596.3
Database[h]	87.25	172.50	83.92	168.52	1.1282	1.1842	2223.7	1276.5	589.2[i]

[a]Dissociation energies ((D_0) includes the zero-point vibrational energy correction) to give $O(^1D)+N_2$ and $N(^2D)+NO$, respectively.

[b]Masses of the most abundant isotopes are used: ^{14}N and ^{16}O. The harmonic frequencies ω_i for normal modes are shown ordered by symmetry: Σ^+, Σ^+, Π.

[c]Reference 14.

[d]Reference 33.

[e]Reference 41. D_e is derived by means of the experimental N_2 zero-point energy (ZPE) from Table I.

[f]Reference 38.

[g]Reference 27.

[h]Reference 1. Dissociation energies are derived from the $\Delta_f, H^0_{0\,K}$ values and the experimental vibrational frequencies. The D_0 values are coincident with the photolysis data reported in Ref. 58.

[i]Fundamentals ν_i frequencies.

TABLE IV. A comparison of different *ab initio* data on cyclic-C_{2v} and $D_{\infty h}$ isomers of N_2O.

Linear NON($^1\Sigma_g^+$, MIN 5)	E (kcal/mol)[a]	$R_{e\,(NN)}$ (Å)	$R_{e\,(NO)}$ (Å)	N_oN (°)	ω_i[b] (cm^{-1})		
SCF/Whitten's basis[c]	117.59	2.40	1.20	180	-	-	-
SCF/6-31G(d)[d]	157.1	2.28	1.14	180	2067	1499	663
MP2/6-311++G(d)[e]	66.63	2.684	1.342	180	2398	546	368
CCSD(T)/TZ-ANO[f]	110.67	2.404	1.202	180	-	-	-
BD(T)/cc-pVTZ[g]	111.1	2.406	1.203	180	1838	1105	485
CASPT2(16,12)/ 6-311G(2d) (this work)	107.64	2.4256	1.2128	180	1695.7	1056.4	434.4
Cyclic NON($^1A_1$, MIN 7)							
MCSCF/DZ[h]	58.80	1.2	1.6	43.6	-	-	-
MP2/6-311++G(d)[e]	75.72	1.214	1.511	47.4	1636	966	287
CCSD(T)/TZ-ANO[f]	64.91	1.188	1.536	45.4	-	-	-
BD(T)/cc-pVTZ[g]	64.4	1.190	1.531	45.7	1779	839	376
CASPT2(16,12)/ 6-311G(2d) (this work)	66.65	1.2054	1.5487	45.3	1731.0	757.2	303.2

[a]Relative energy with respect to the NNO molecule.
[b]Masses of the most abundant isotopes are used: ^{14}N and ^{16}O. The harmonic frequencies ω_i for normal modes are shown ordered by symmetry: Σ_u^+, Σ_g^+, $\Pi_u(D_{\infty h})$ or A_1, A_1, $B_1(C_{2v})$.
[c]Reference 34. The NO distance was kept fixed at 1.20 Å.
[d]Reference 35.
[e]Reference 36.
[f]Reference 37.
[g]Reference 38. Energy with the Brueckner Doubles method with a perturbative correction for triples: BD(T)/aug-cc-pVTZ//BD(T)/cc-pVTZ level.
[h]Reference 14. Energy at the MCSCF/DZ+d level.

cies were converged with an uncertainty lower than 3%, which was estimated with several fittings. A comparison of the results presented in Table III reveals that the CASPT2 data give a very good overall behavior of these properties, improving significantly the dissociation energies with respect to previous *ab initio* studies. The energy differences with respect to the experimental data are lower than 2.5 kcal/mol (i.e., relative errors less than 1.5% or 3% for D_e or D_0 values). Previous theoretical attempts to determine dissociation energies are relatively scarce and mostly concentrated on the channel (1) [i.e., $O(^1D)+N_2(X\,^1\Sigma_g^+)$] as one can notice from Table III.

The existence of some of the reported minima has been noted previously, as explained in the Introduction. Apart from the N_2O molecule, a linear NON minimum was found in an old study by Peyerimhoff and Buenker[34] and in later studies as well.[35–38] The electronic configuration for this minimum is $(1-4\sigma_g)^2(1-3\sigma_u)^2(1\pi_u)^4(1\pi_g)^4$ in $D_{\infty h}$ symmetry. In the first work,[34] a SCF method with Whitten's fixed group Gaussian type basis set[59] was employed reaching an energy lying about 117.59 kcal/mol above the lower N_2O minimum (its geometry was kept fixed at $R_{e(NO)}=1.20$ Å for NON, and at $R_{e(NN)}=1.126$ Å and $R_{e(NO)}=1.191$ Å for N_2O). Table IV summarizes the results of all mentioned studies and show our results. The present calculations for the MIN 5 yield a N–O distance of 1.2038 and 1.2128 Å and a relative energy of 112.74 and 107.64 kcal/mol at the CASSCF and CASPT2 levels, respectively, in very good accordance with the previous best quality *ab initio* [i.e., CCSD(T)[37] and BD(T)[38]] data.

A cyclic-C_{2v} ($^1A_1$) minimum in the ground PES was first noticed by Hopper[14] in its extensive study of the electronic spectrum of N_2O. At the MCSCF level with a basis set of double-zeta quality, this author found this minimum to present $R_{e(NN)}=1.2$ Å and $R_{e(NO)}=1.6$ Å equilibrium distances, which was 58.80 kcal/mol above the N_2O molecule. This minimum corresponds to our reported MIN 7. More recent works have also dealt with this cyclic isomer.[36–40] In Table IV are summarized the most significant previous *ab initio* data and are compared with our CASPT2 results; these are in almost quantitative agreement for all properties with respect to the preceding high level *ab initio* studies. The main electronic configuration of this minimum is $(1-2a_1)^2(1b_1)^2(3-4a_1)^2(2b_1)^2(1b_2)^2(5-6a_1)^2(3b_1)^2(2b_2)^2$ in C_{2v} symmetry. Full coincidence is found in the relative energy ordering of the three N_2O minima: $NNO(^1\Sigma^+)<$cyclic-$C_{2v}NON(^1A_1)<NON(^1\Sigma_g^+)$.

There is little *ab initio* information on the energy barriers among the above-mentioned NNO isomers. Values of about 26 and 53 kcal/mol were reported, respectively (geometries were not indicated) at MP2/6-311++G(d) level[36] for the cyclic-C_{2v} NON isomer to produce the NNO molecule or the NON isomer. The calculated CASPT2 energy barriers are 14.80 (TS 9) and 64.66 (TS 5) kcal/mol, respectively. The differences between both studies should be expected as it was previously pointed out that the MP2/6-311++G(d) method with a frozen core approximation and with a minimal polarized basis set did not allow sufficient variational freedom in the calculations to describe properly the energy of these isomers,[37] giving place to a reverse prediction in their stability.

TABLE V. Location and energetics of the ($1\,^1A'$,$2\,^1A'$) surface crossing.[a]

	CAS (8, 6)		CAS (10, 8)		CAS (16, 12)[e]	
$R_{(NN)}$ (Å)	1.1596		1.1988		-	
$R_{(NO)}$ (Å)	1.3614		1.3796		-	
∠NNO (deg)	110.9		108.2		-	
ΔE (kcal/mol)[b]	0.149	0.934	0.065	1.267	6.226	5.640
$1\,^1A'$: C_i (CSFs)[c]	0.936	−0.101	0.079	0.894	−0.018	0.898
Reference weight[d]	0.830		0.894		0.913	
$2\,^1A'$: C_i (CSFs)[c]	0.106	0.914	0.916	−0.068	0.917	0.025
Reference weight[d]	0.871		0.873		0.911	

[a]Calculations at the CASSCF/6-311G(2d) level with different complete active spaces [CAS (*e*-, orb.)]. The CASPT2 energies are calculated at the CASSCF optimal geometry.

[b]Energy difference between the ground and the first excited $^1A'$ surfaces at the conical intersection: CASSCF (first value) and CASPT2 (second value).

[c]Coefficients (C_1, C_2) of the two most important CSFs in the CASSCF wave function: CSFs ($3a'$, $3a''$) for CASSCF (8,6): (211 220) (220 220); CSFs ($5a'$, $3a''$) for CASSCF (10, 8): (22110 220) (22200 220).

[d]Weight of the CASSCF reference function in the total CASPT2 wave function.

[e]Calculation at the CASSCF (10, 8)/6-311G(2d) geometry.

C. $1\,^1A'/2\,^1A'$ surface crossings

A seam of conical intersection or avoided crossing between the fundamental $^1A'$ and the first excited $2\,^1A'$ surfaces has been investigated using a direct algorithm[60] as implemented in the GAUSSIAN 98 code.[44] The two states implied were given a weight of 50% in the state-averaged CASSCF wave function. A reduction of the active space with respect to the full valence one had to be performed for practical reasons, although at the same time the smaller active spaces were designed to include the important chemistry of the system in the crossing zone. Two active spaces, CAS (8,6) and CAS (10,8), were considered in the search of the intersection. In the obtained crossing point, the two potential surfaces were separated by about only 0.15 and 0.07 kcal/mol at the state-averaged CASSCF level, respectively, as shown in Table V; the geometries were also very close to each other. The dominant electronic configurations correspond to the RHF N_2O closed-shell configuration ($1\,^1A'$) and a single excitation to the first virtual a' orbital ($2\,^1A'$). However, the ordering of the states is inverted in the point located with the (8,6) active space. To determine the extent to which the geometry of the located points depends on the increase in size of the active space, pointwise calculations with active spaces augmented to include all the $2p$ electrons [i.e., CAS (10,9)] and with the full valence active space [i.e., CAS (16,12)] were subsequently done at the optimal point. A summary of these results is presented in Table V. One can notice that there is a small increase in the energy gap (ΔE) between the potential surfaces whenever one of the augmented active spaces is used. The point located with the (10,8) active space seems to be closer to the hypothetical (10,9) and (16,12) crossing points, particularly for this last one. However, the CASPT2 results obtained with the smaller active spaces should be regarded with caution because of the lesser magnitude of the reference weight and its different value for each of the electronic states considered. The energy differences found in this region could reflect the sharp variation of the electronic energy with respect to the nuclear coordinates in the crossing zone. Moreover, a more accurate search of the geometry at the CASPT2 level could modify slightly the geometry and hence also ΔE values.

The existence of several crossings between the lowest singlet and triplet adiabatic potential energy surfaces of the N_2O system correlating with $N_2+O(^1D, ^3P)$ have been studied in several preceding works.[14,42,61] However, little information was reported for the ($1\,^1A'$,$2\,^1A'$) intersection studied in the present work. Hopper's work[14] allows to locate this intersection in the region $R_{(NN)}=1.13$ Å, $R_{(NO)}=1.18$ Å (distances not optimized) and ∠NNO≈105° with $\Delta E\approx 6.3$ kcal/mol at MCSCF-CI/DZ level. In a recent paper, Jimeno *et al.*[60] found that there was an avoided crossing between these surfaces in the region $R_{(NN)}=1.13$ Å (kept fixed), $R_{(NO)}\leqslant 1.45$ Å (partially optimized) and ∠NNO ≈87° (partially optimized), with $\Delta E\leqslant 11.5$ kcal/mol at the MRCI(10,9)+Q/aug-cc-pVDZ level and 0.02 kcal/mol at the CASSCF (10,9)/aug-cc-pVDZ level. The latter authors suggest that this avoided crossing can give rise to a seam of conical intersections at other NN separations. Our results (Table V) are in close agreement with these studies although our location of this intersection is more precise. On the other hand, the fact that two surfaces of the same symmetry (spin and space) can cross is in accordance with many studies found in the literature (see, for example, Refs. 62–63). The noncrossing rule applies only to diatomic molecules, whereas for a polyatomic molecule there can exist a seam of conical intersection of dimension $M-2$, where M is the number of independent nuclear coordinates for the molecular symmetry considered. Therefore, for the NNO system keeping C_s symmetry one has $M=3$ independent internal coordinates and consequently it is feasible to have a one-dimensional seam of conical intersection (i.e., a line). However, the algorithm employed here only permits the location of the minimum energy point in the line of intersection between the two lowest $^1A'$ surfaces. The reduced energy gap between the two electronic states found in the present study seems to point towards a conical intersection rather than an avoided crossing between the surfaces. However, the dimensionality rules explained above do not guarantee the surfaces to cross, the crossing being only allowed by them. Further treatment of the problem would imply the study of the NNO geometries placed on the line of intersection, but deeper insight into this question is beyond the scope of this study.

The very good results obtained for reactants and products of reaction (8) along with those for the N_2O isomers and the ($1\,^1A'$,$2\,^1A'$) surface intersection, when compared with preceding *ab initio* data and with available experimental data, point towards the suitability of describing the ground $^1A'$ NNO PES at the CASPT2(16,12)/6-311G(2d) level of theory.

III. ANALYTICAL GROUND $^1A'$ PES

An extensive grid of *ab initio* CASPT2 points (about 1250) of the ground $^1A'$ surface have been fitted to a suitable analytical function to provide a smooth continuous variation of the energy with respect to the nuclear coordinates. To this aim, we have used an NN′O Sorbie–Murrell many-body expansion, i.e., one that consists in a sum of one-, two- and three-body terms:[64]

$$V(R_1,R_2,R_3)=V^{(1)}_{\mathrm{N}(^2D)}\cdot f_1(R_1,R_2,R_3)+V^{(1)}_{\mathrm{N}'(^2D)}\cdot f_2(R_1,R_2,R_3)+V^{(1)}_{\mathrm{O}(^1D)}\cdot f_3(R_1,R_2,R_3)+V^{(2)}_{\mathrm{NN}'}(R_1)+V^{(2)}_{\mathrm{N}'\mathrm{O}}(R_2)+V^{(2)}_{\mathrm{NO}}(R_3)+V^{(3)}_{\mathrm{NN}'\mathrm{O}}(R_1,R_2,R_3), \tag{12}$$

where $V^{(1)}$, $V^{(2)}$ and $V^{(3)}$, are the one-, two- and three-body terms, respectively, and R_1, R_2 and R_3 represent the NN′, N′O and NO distances, respectively. As the diatomic molecules dissociate in atoms in their ground state [i.e., N(^4S) and O(^3P)] but in reactants and products of reaction (8) the excited atoms are present [i.e., N(^2D) and O(^1D)], an accurate representation of the PES will be at least two-valued [i.e., $\mathrm{N}(^4S)+\mathrm{N}(^4S)+\mathrm{O}(^1D)$ and $\mathrm{N}(^2D)+\mathrm{N}(^4S)+\mathrm{O}(^3P)$ limits]. In order to get a simple analytical form for the PES we have used a single-valued representation that reproduces properly the two atomic states in the reactants and products asymptotes. Thus, the one-body terms consist of products of the energy of the excited atoms relative to their fundamental states and switching functions f_i, whose values range between 0 and 1,

$$f_i(R_1,R_2,R_3)=\frac{1}{2}\left[1-\tanh\frac{\alpha_i S_i'}{2}\right],\quad i=1,\ 2,\ 3, \tag{13}$$

where S_i' are expressed in terms of displacement coordinates ($\rho_j=R_j-R_j^0$) with respect to a C_{2v}-NON reference structure (i.e., $R_1^0,R_2^0=R_3^0$), thereby introducing the correct symmetry of the PES with respect to the N–N′ interchange:

$$S_i'=\sum_{j=1}^{3} b_{ij}'\rho_j,\quad i=1,\ 2,\ 3. \tag{14}$$

These one-body terms assure the correct asymptotic limits for reaction (8). The adjustable parameters α_i were partially optimized in the global fitting of the PES. These switching functions do not assure that a unique value of the energy is obtained for all the geometries of the system in which the three atoms are far away from each other, but only for most of them by using the b_{ij}' parameters shown in Table VI. Nevertheless, this uniqueness is not crucial for the study of reaction (8) because the three atomic regions will not be explored at all at the energy conditions defined in the present study.

The two-body terms (diatomic potential energy curves) have been fitted using extended-Rydberg potentials up to fifth order,

$$V^{(2)}(R_i)=-D_{e(i)}\left(1+\sum_{j=1}^{n=5} a_{ij}\rho_i^j\right)e^{-a_{i1}\rho_i},\quad i=1,\ 2,\ 3, \tag{15}$$

where $\rho_i=R_i-R_i^e$, and $D_{e(i)}$ and R_i^e are the dissociation energy and the equilibrium bond length of the corresponding ''i'' diatomic molecule, respectively. Sets of 65 and 62 CASPT2 points were generated for the N_2 and NO molecules, respectively, and were fitted by means of a nonlinear least-squares method[65] providing excellent results in both cases [root-mean-square deviation (RMSD) below 0.3 kcal/mol]. The optimal values of the a_{ij} parameters are given in Table VI.

The three-body term is constructed as the product of an n-order polynomial expressed in terms of the S_i coordinates [as in Eq. (14) for S_i' but now with the b_{ij} parameters shown in Table VI] and a range function $T(S_1,S_2,S_3)$ which cancels out the three-body term whenever one atom is separated from the other two,

$$V^{(3)}_{\mathrm{NN}'\mathrm{O}}(R_1,R_2,R_3)=P(S_1,S_2,S_3)\cdot T(S_1,S_2,S_3), \tag{16}$$

where

$$P(S_1,S_2,S_3)=\sum_{i,j,k=0}^{0<i+j+k<n} C_{ijk}S_1^iS_2^jS_3^k, \tag{17}$$

with i, j and k positive integer numbers, and

$$T(S_1,S_2,S_3)=\prod_{i=1}^{3}\left[1-\tanh\frac{\gamma_i S_i}{2}\right]. \tag{18}$$

The number of parameters in the three-body term is reduced owing to the use of the permutational symmetry. From the set of linear $\{C_{ijk}\}$ and nonlinear $\{\gamma_i\}$ parameters those which are associated to odd powers of S_3 (which is antisymmetric with respect to the interchange of the nitrogen atoms) are identically zero. The nonzero parameters are determined by a nonlinear least-squares procedure[66] in which the energies and geometries of a set of CASPT2 points are given as data. The weights of the different points can be varied in order to privilege a certain portion of the information introduced into the fit. A global fit of the information obtained on the NNO and NON zones of the $^1A'$ PES to the three-body term of the Sorbie–Murrell expansion was performed. This PES is, in principle, suitable for the study of the dynamics of reaction (8). The whole set of *ab initio* points (a total of 814 points within the NNO regions and 307 points with the NON regions) was fitted to a sixth degree of the polynomial with all their weights equal to 1.0 except for the reactants entrance zone. For this one, a weight of 10.0 was given to the points located around TS 4 to assure a correct energy barrier, and a weight of 5.0 to the geometries situated in the very entrance N··NO zone, so as to eliminate a spurious TS with an energy

TABLE VI. Optimal parameters for the fitted analytical $^1A'$ PES.[a]

One-body terms

$V^{(1)}_{N(2D)}$ (eV)	$V^{(1)}_{O(1D)}$ (eV)	α_1 (Å^{-1})	α_2 (Å^{-1})	α_3 (Å^{-1})
2.6730	2.1133	1.5	1.5	1.0

b'_{ij} (Å^{-1}), $i,j=1,\ 2,\ 3$

−1.0	3.0	−1.0
−1.0	−1.0	3.0
3.0	−1.0	−1.0

Two-body terms

	a_1 (Å^{-1})	a_2 (Å^{-2})	a_3 (Å^{-3})	a_4 (Å^{-4})	a_5 (Å^{-5})
N_2	3.88769	0.10039	−0.91232	−2.73055	1.69645
NO	4.14169	0.85873	−0.97298	−3.70379	2.48770

Three-body term

(ijk)	C_{ijk} (eV·Å$^{-(i+j+k)}$)	(ijk)	C_{ijk}	(ijk)	C_{ijk}	(ijk)	C_{ijk}	(ijk)	C_{ijk}
000	−0.24433	102	−134.14	022	35.162	104	158.48	240	93.839
100	16.969	030	7.2390	004	103.78	050	1.8731	222	5.9270
010	4.8575	012	43.378	500	−54.518	032	17.021	204	112.29
200	56.034	400	55.661	410	176.68	014	−59.694	150	14.640
110	−18.508	310	221.50	320	150.76	600	15.195	132	−106.10
020	−4.0797	220	−23.899	302	−312.04	510	−78.309	114	113.15
002	−38.106	202	−177.70	230	14.073	420	3.6847	060	−1.9621
300	183.29	130	49.853	212	−179.41	402	82.405	042	41.761
210	58.689	112	17.935	140	51.178	330	56.899	024	−28.755
120	−48.634	040	−4.0670	122	56.321	312	−204.17	006	−74.606

R^0_1 (Å)	$R^0_2=R^0_3$ (Å)	γ_1 (Å^{-1})	γ_2 (Å^{-1})	γ_3 (Å^{-1})
1.1343	2.0000	2.8996	2.9310	0.0

b_{ij} (Å^{-1}), $i,j=1,\ 2,\ 3$

1.0	0.0	0.0
0.0	$\sqrt{1/2}$	$\sqrt{1/2}$
0.0	$\sqrt{1/2}$	$-\sqrt{1/2}$

[a]The diatomic dissociation energies and equilibrium distances used in the fit are given in Table I.

above reactants that is present in the fitted PES if the weights in this zone are given a value equal to 1.0. The optimal linear ($N=50$) and nonlinear ($N=2$) parameters for the fitted PES as well as the reference structure (partially optimized) are presented in Table VI. A global RMSD of 1.12 kcal/mol was obtained, its value being 0.96 kcal/mol for the NNO zone and 1.48 kcal/mol for the NON zone. This potential surface is completely *ab initio* in nature since agreement with experimental data was not looked for. In Table VII all the stationary points located are presented. They are also depicted along with their relative energies in Fig. 2.

For the N_2O molecule, a comparison between the results given in Tables III and VII reveals that the corresponding N–N and N–O equilibrium distances are about as accurate in both cases [i.e., they are deviated 0.008, 0.010 Å from the experiment in the local fit (Table II) and 0.005, 0.015 Å in the global potential surface (Table VII), respectively]. On the other hand, the dissociation energies are very alike in both cases, which was to be expected because of the minor differences in the equilibrium geometry. Finally, the fitted PES tends to underestimate slightly the N_2O stretching frequencies, giving an almost correct value for the bending mode. In addition to the harmonic frequencies, the three first IR bands of Σ symmetry were calculated by means of the TRIATOM program[67] which is based on the diagonalization of the rovibrational matrix in a certain basis set. We chose to represent the vibrational motion in a basis set composed by 12 and 7 Morse-like basis functions for the NN and NO stretching vibrations, respectively, with parameters $D_e=169.4$, 87.8 kcal/mol; $\omega_e=2194.7$, 1316.8 cm^{-1}; and $R_e=1.1329$, 1.1990 Å, respectively. For the description of the bending motion associated, Legendre polynomials to the 74th-order were employed. The lowest 3500 basis functions were kept for the final diagonalization of the Hamiltonian. The resulting values, 2151.8, 1254.0 and 1168.9 cm^{-1} for the (100), (010) and (002) bands, respectively, should be compared to the experimental results, i.e., 2223.8, 1284.9 and 1168.1[16–18] [normal modes are ordered as: Σ^+(NN str.), Σ^+(NO str.), Π(bend)]. Therefore, the two fundamentals and the (002) band show the same tendency as the harmonic frequencies, the bending motion being the best represented by the PES.

A comparison can be established between the stationary points located in the analytical PES and the original, locally fitted CASPT2 points (i.e., compare Tables II and VII on the one hand, and Figs. 1 and 2 on the other). First, two of the structures (the points labeled TS 5 and MIN 6) are not reproduced by the fit. A possible explanation could be given by CASPT2 fits (Table II) in this zone, which indicate a marked resemblance in both geometry and energy for TS 5, MIN 6 and TS 6. By any means, this zone is not expected to be of

TABLE VII. Properties[a] of the stationary points on the analytical $^1A'$ PES.

Symmetry/ stationary point	Energy (kcal/mol)	$R_{e\,(NN)}$ (Å)	$R_{e\,(NO)}$[b] (Å)	α[c] (°)	ω_i[d] (cm^{-1})		
			$C_{\infty v}$				
MIN 2 (NNO)	−170.90	1.1326	1.1999	180.0	2216.5	1250.2	589.7
			$C_{2v}, D_{\infty h}$				
MIN 5	−63.78	2.3237	1.1618	180.0	2041.8	894.1	245.3
MIN 7	−104.60	1.1558	1.5887	42.7	1745.7	913.7	682.5
MIN 8	−86.31	1.1170	2.7413	23.5	2153.4	168.9	146.1
TS 6	−45.70	1.7843	1.3171	85.3	1254.0	518.6i	1018.1
TS 7	−82.49	1.1100	2.1379	30.1	2174.7	385.6i	410.1
			C_s				
MIN 1	−0.65	3.3471	1.1590	158.4	1847.7	64.3	23.0
MIN 3	−87.37	1.1109	2.8191	131.3	2306.8	184.2	103.8
MIN 4	−5.05	3.1981	2.7543, 1.1468	102.1	1855.9	293.4	232.2
TS 1	−0.46	2.8792	1.1554	140.7	1815.6	103.7	94.6i
TS 2	−86.34	1.1027	2.3869	150.6	2335.5	122.8	195.3i
TS 3	−0.13	3.7490	1.1574	93.6	1852.2	38.1	70.1i
TS 4	1.91	2.9979	2.1367, 1.1672	129.9	1709.8	201.6	418.0i
TS 9	−90.46	1.1347	1.4029	97.6	1986.3	810.2	744.7i

[a]Energies are given relative to reactants [i.e., $N(^2D)+NO$].
[b]Both NO distances are reported for NON (C_s) structures.
[c]α is the ∠NON angle for C_{2v}, $D_{\infty h}$ and NON (C_s) structures or ∠NNO otherwise.
[d]Masses of the most abundant isotopes are used; ^{14}N and ^{16}O. The order of the harmonic frequencies for normal modes is as follows: Σ^+, Σ^+, $\Pi(C_{\infty v})$; Σ_u^+, Σ_g^+, $\Pi_u(D_{\infty h})$; A', A', $A'(C_s)$ or A_1, A_1, $B_1(C_{2v})$. Frequencies for equal symmetry modes are shown in decreasing order with the imaginary one at the end.

major relevance to the dynamics of the system. The analytical fit predicts also the existence of a new stationary point (i.e., TS 1) which is situated in the very entrance N··NO channel, although it is situated energetically below reactants. The analytical fit shows a tendency to give this TS, and we believe that a more accurate search at the CASPT2 level would give also this loose structure. With the above-mentioned exceptions, the stationary points which are common to Figs. 1 and 2 show rather similar geometries and relative energies within the PES, though the frequencies are only reproduced in a qualitative way. However, one must bear in mind that the local fits presented in Table II have their own intrinsic errors, which are more important for the frequencies than for the other two properties.

A picture of the general aspect of the analytical PES in the zone containing MIN 2 (NNO molecule) is provided in Fig. 3. Figure 4 shows clearly the presence of MIN 4, TS 4, and MIN 5 (linear NON isomer). The energy contours for the insertion of the oxygen atom perpendicularly to the N–N bond (C_{2v} symmetry) which reproduce the portion of the

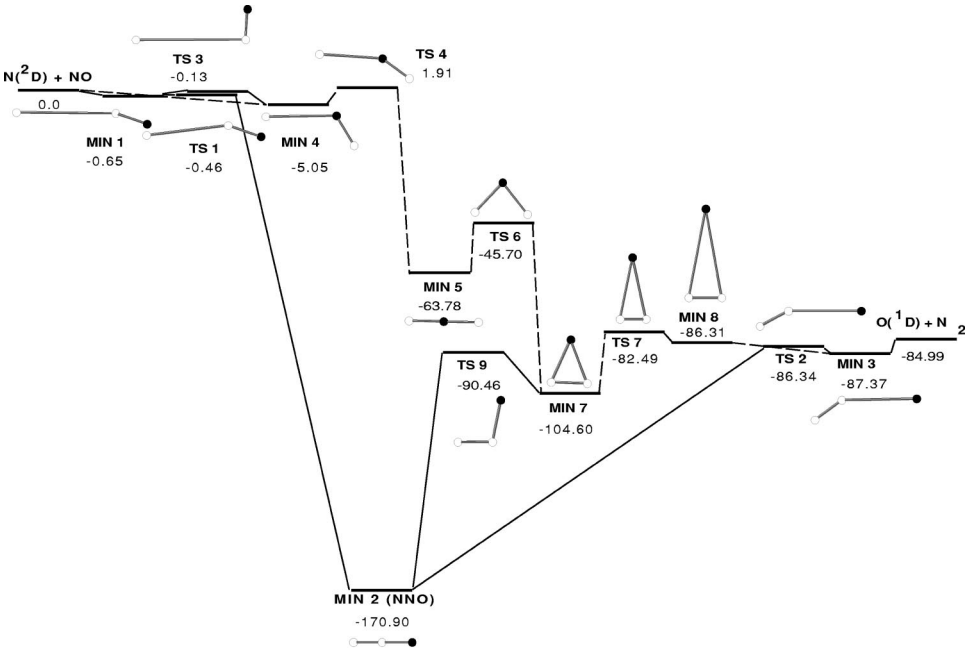

FIG. 2. Energy diagram of the stationary points located on the analytical Sorbie–Murrell $^1A'$ PES. Energies are given relative to reactants, $N(^2D)+NO$, in kcal/mol.

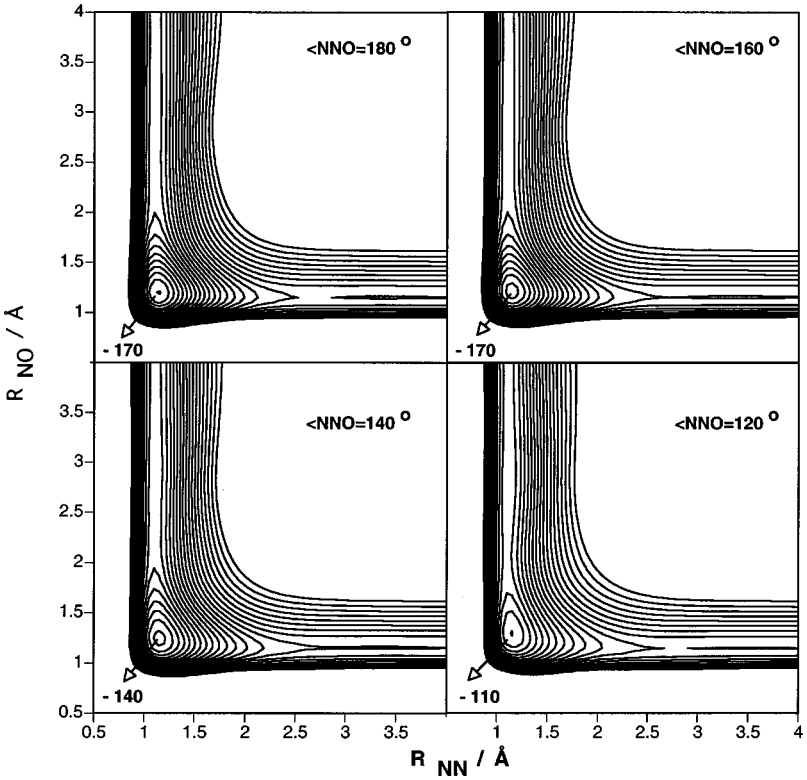

FIG. 3. Contour diagrams of the analytical $^1A'$ PES at different $\angle$NNO angles. The contours are depicted in increments of 10 kcal/mol and the zero of energy is taken in reactants [i.e., $N(^2D+NO)$].

PES linking the MIN 5 minimum to products, $O(^1D)+N_2$, are displayed in Fig. 5.

Finally, the zone situated between NNO and MIN 7, in which a crossing between the two first $^1A'$ surfaces has been found (see above), is more difficult to describe. As a consequence, the structure of TS 9 and its energy barrier are subject to some uncertainty, as indicated by the relatively high errors in geometry and frequencies (see above) even though the related properties are in accordance for the local and the global fit.

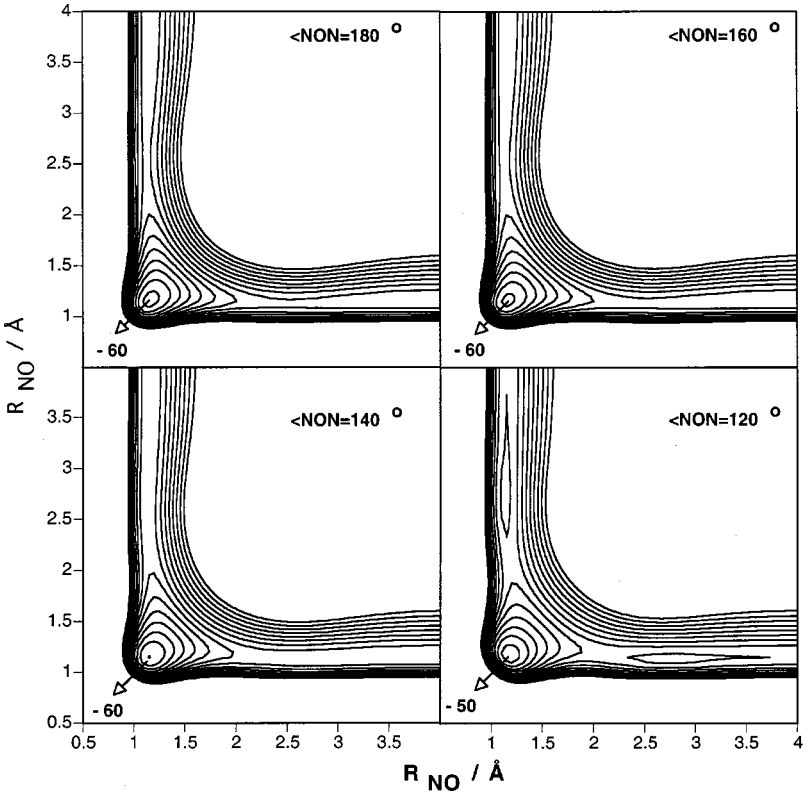

FIG. 4. Contour diagrams of the analytical $^1A'$ PES at different $\angle$NON angles. The contours are depicted in increments of 10 kcal/mol and the zero of energy is taken in reactants [i.e., $N^2(D+NO)$].

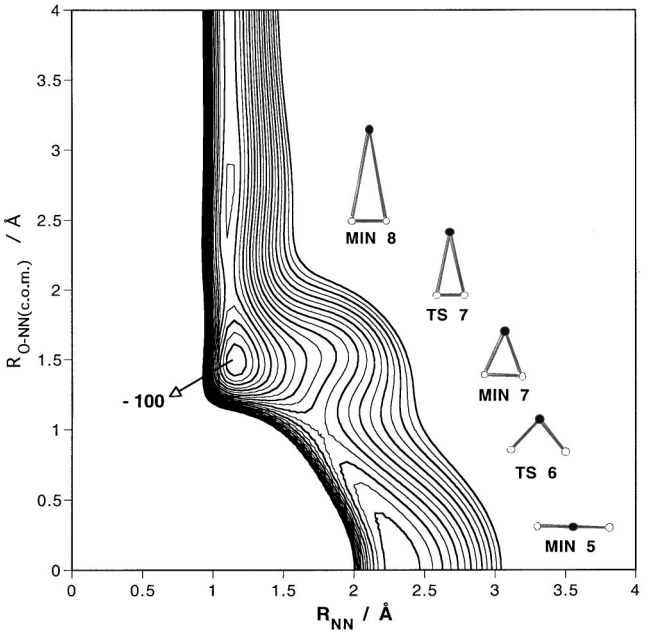

FIG. 5. Contour diagrams of the analytical $^1A'$ PES for the insertion of the oxygen atom into the N–N bond in C_{2v} symmetry. $R_{\mathrm{O-NN(c.o.m.)}}$ represents the distance to the center of mass of the NN molecule. The contours are depicted in increments of 5 kcal/mol and the zero of energy is taken in reactants [i.e., $\mathrm{N}(^2D)+\mathrm{NO}$].

IV. THERMAL RATE CONSTANTS AND REACTION DYNAMICS

A. Quasiclassical trajectory method

The analytical *ab initio* ground $^1A'$ PES constructed above has been employed to perform a quasiclassical trajectory (QCT) study. Thus, theoretical thermal rate constants were calculated and compared with the available experimental data. Also, vibrational and rovibrational distributions, among other reaction properties, were determined and related to the microscopic mechanism of reaction. The QCT calculations have been carried out by means of a computational code developed in our laboratory.[68] The accuracy of the numerically integrated trajectories was checked according to the energy and angular momentum conservation criteria. The integration step size chosen (i.e., 5×10^{-17} s) was found to achieve these conservation requirements for all the calculated trajectories. The trajectories were started and finished at a distance from the atom to the center of mass of the corresponding diatomic of about 8.0 Å, thus ensuring that the interaction between the fragments was negligible. A standard Monte Carlo sampling[69] of the initial conditions following a Maxwell–Boltzmann distribution of both the translational and rovibrational energy ($T_{\mathrm{trans}}=T_{\mathrm{vib-rot}}=300,500,1000,1500$ K) yielded directly the thermal reaction cross-sections. Approximate final quantized internal distributions [i.e., $P(v')$ and $P(v',J')$] were obtained from rotational and vibrational radial action variables[70] by a histogram method. A total of about 30 000 trajectories for $T=300$ K, and 10 000 for the other temperatures, was considered sufficient in order to obtain a low statistical deviation for all the studied properties. In particular, an error lower than 3% was obtained for the total reaction cross-sections of reaction (8).

B. Kinetical properties

As it was indicated in the Introduction, experimental information on the studied reaction is scarce, concerning only the total $\mathrm{N}(^2D)+\mathrm{NO}(X\,^2\Pi)$ rate constant at room temperature (around 300 K). Thus, a direct comparison between the calculated and experimental rate constants is not feasible, the latter being a possible upper estimate of the rate constant for the reaction (8). The obtained QCT rate constant was corrected for a statistical factor of $\frac{1}{40}$, which reflects the number of microstates arising from reactants, $\mathrm{N}(^2D)+\mathrm{NO}(X\,^2\Pi)$, and the fact that we have considered in a first approximation that the ground $^1A'$ PES could account for the total reactivity of the system. In this way a value of $(2.63\pm0.07)\times10^{-12}\,\mathrm{cm^3\,molecule^{-1}\,s^{-1}}$ was obtained substantially lower than the total experimental rate constant [i.e., from $(3.5\pm0.3)\times10^{-11}\,\mathrm{cm^3\,molecule^{-1}\,s^{-1}}$ [12] to $(8.3\pm0.3)\times10^{-11}\,\mathrm{cm^3\,molecule^{-1}\,s^{-1}}$ (Ref. 13)]. We have tried to take into account in some way the reactivity due to the other four excited PESs connecting with products (i.e., $2\,^1A',3\,^1A',1\,^1A'',2\,^1A''$). To this aim, we have calculated the energies of these states in selected points of an approximate MEP in the entrance NNO zone of the analytical ground PES, comprising the TS 1 stationary point. Equally weighted state-averaged CASSCF(16, 12) wave functions were constructed separately for the three $^1A'$ PESs and for the two $^1A''$ PESs, and CASPT2 calculations were performed on each one of them. The results for the energies with respect to reactants corresponding to the TS 1 geometry are as follows: -0.40, -0.17, 0.07, 0.61 and 0.76 kcal/mol; whereas the energy maxima in the MEP are situated at -0.34, 0.43, 3.07, 6.13 and 7.01 kcal/mol, with a state ordering $1\,^1A'$, $2\,^1A'$, $1\,^1A''$, $2\,^1A''$ and $3\,^1A'$, respectively. Therefore, at a temperature of 300 K one could expect that at least the two first $^1A'$ PESs, whose barriers are below 1 kcal/mol, would contribute significantly to the reactivity. It is doubtful whether the next $1\,^1A''$ PES would be relevant or not in this context. However, the MEP on which the calculations are based corresponds to the $1\,^1A'$ PES of the system, and the shift of the geometry and the energy of the TS for each excited electronic state has not been investigated by using different one electron basis sets and the CASPT2 method. For these reasons, the real barrier could be considerably lower if these effects had been taken into account. In conclusion, the rate constant for reaction (8) could reasonably be within the range $2.6\times10^{-12}\,\mathrm{cm^3\,molecule^{-1}\,s^{-1}}$ (only $1\,^1A'$ PES) to $7.9\times10^{-12}\,\mathrm{cm^3\,molecule^{-1}\,s^{-1}}$ (with $1\,^1A',2\,^1A',1\,^1A''$ PESs, assuming a similar contribution of each PES to the total rate constant). We note that the latter value is yet about one fifth of the lowest experimental value reported for the total $\mathrm{N}(^2D)+\mathrm{NO}(X\,^2\Pi)$ rate constant.[12] As stated in the Introduction, the total experimental rate constant is a sum of the rate constants of every process that can be responsible for the depletion of $\mathrm{N}(^2D)$. In particular, it is also expected that rate constants of reactions (7) and (9), through their $^1A'$ and

TABLE VIII. QCT calculated properties on the $N(^2D)+NO$ reaction[a] through the $1\,^1A'$ PES at several temperatures.

QCT properties[b]	T (K) 300	500	1000	1500
b_{max} (Å):				
channel (8)	6.00	5.13	4.59	4.47
channel (6b)	2.70	2.43	3.57	3.29
σ_r (Å)				
channel (8)	12.92±0.21	11.07±0.30	12.03±0.28	11.89±0.29
channel (6b)	0.023±0.011	0.010±0.005	0.25±0.04	0.37±0.04
$k_8(10^{-12}\,cm^3\,molecule^{-1}\,s^{-1})$[c]	2.63±0.04	2.92±0.08	4.48±0.11	6.06±0.12
Branching ratio:				
$k_{(6b)}/(k_{(6b)}+k_{r(8)})$ (%)	0.18	0.090	2.04	3.02
f/b ratio[d]	0.36	0.59	0.91	1.08
$\langle E_{tot}\rangle$ (kcal/mol)[e]	89.29±1.08	90.86±1.84	94.32±3.92	98.70±6.00
$\langle f'_V\rangle$	0.41±0.20	0.46±0.22	0.47±0.24	0.48±0.23
$\langle f'_R\rangle$	0.059±0.07	0.074±0.10	0.13±0.16	0.17±0.18
$\langle f'_T\rangle$	0.54±0.20	0.46±0.22	0.40±0.23	0.35±0.22
Mode of reaction (8):				
route 1 %	96	88	70	53
route 2+3 (%)	4	12	30	47

[a]Reaction channels: $N(^2D)+N'O(X\,^2\Pi)\rightarrow N'(^2D)+NO(X\,^2\Pi)$ (6b); $\rightarrow O(^1D)+NN'(X\,^1\Sigma_g^+)$ (8).
[b]30000 trajectories calculated at 300 K and 10000 otherwise. Errors show one standard deviation.
[c]Statistical multiplying factor equal to 1/40 (only $^1A'$ PES) is included in the reported k_8 values. The QCT values are well reproduced by the analytical fit: $k_8=2.98\times10^{-15}T^{1.01}e^{297/T}\,cm^3\,molecule^{-1}\,s^{-1}$.
[d]Forward ($\theta'<90°$) / backward ($\theta>90°$) ratio.
[e]Mean total energy and mean of the energy fractions (E'_1/E_{tot}) for each I' energy [i.e., vibration (V'), rotation (R') and translation (T')] at each temperature.

$^3A''$ PESs, respectively, could provide a large extent to the overall rate constant (i.e., $k\approx k_7+k_8+k_9$, as much lower values for k_6 and k_{10} are expected).

Despite the goal of the present work was to study the reaction (8) and not the total $N(^2D)+NO$ reaction, an additional study on the reaction (9) was also begun, and it is now in progress. As this latter reaction is the most exothermic process among the $N(^2D)+NO$ reaction channels, and will have a statistical factor of 3 (i.e., $^3A''$ PES) in the total rate constant, this could be also important in the total k value. Our preliminary *ab initio* CASSCF/CASPT2 studies, with the same active space and basis set as for reaction (8), reveals the absence of an energy barrier for this reaction. Thus, at the CASSCF(16, 12)/6-311G(2d) level an angular TS (harmonic frequencies $\omega_i=1883.6$, 146.7 and 209.3i cm^{-1}), with $R_{(NN)}=2.4002$ Å, $R_{(NO)}=1.1563$ Å and $\angle NNO\approx116.0°$, and an energy barrier of 1.90 kcal/mol, was found. However, at the CASPT2 level the energy barrier disappears (i.e., $E=-0.69$ kcal/mol at the TS geometry). This results suggest the validity of the assumption made by other authors[15] that reaction (9) should present a similar rate as the analogous $N(^4S)+NO$ reaction,

$$N(^4S)+NO(X\,^2\Pi)\rightarrow O(^3P)+N_2(X\,^1\Sigma_g^+)$$

$$\Delta_r H^0_{0\,K}=-75.01\,kcal\,mol^{-1}, \quad (19)$$

whose experimental value is $(3.0\pm0.8)\times10^{-11}\,cm^3\,molecule^{-1}\,s^{-1}$ at 300 K,[71] and where only the lowest $^3A''$ PES (without an energy barrier) is significant.[72] Hence, the addition of k_9 and also of k_7 (not studied yet) could account for the total $N(^2D)+NO$ rate constant, as the other physical electronic quenching process (10) should be negligible [e.g., as in $N(^2D)+H_2,D_2$ reactions[73]]. A work in progress on the similar $N(^2D)+O_2$ reactions shows also that this latter process is much less important than the other reaction channels.[74] However, Takayanagi *et al.* have recently invoked this kind of process to explain the theoretical results on related $N(^2D)$ reactions [e.g., $N(^2D)+H_2O$,[75] CH_4, CD_4,[76] or C_2H_4 [77]]. Further studies should be needed to clarify this point.

The effect of the temperature on reaction (8) is typical of reactions without a threshold energy. Reaction cross-section increases very little or even decreases (Table VIII) and the rate constants show only a small increase due to the increment of the mean relative velocity of reactants [i.e., $k(T)\approx\sigma_r(T)\cdot\langle v_r\rangle_T$]. However, a significant contribution of the N-exchange reaction (6b) appears also at higher temperatures. This behavior seems to be in agreement with the observed experimental results for the isotopically labeled $^{13}N(^4S,\,^2D,\,^2P)+NO$ reactions at very high kinetic energies. Despite the fact that the N-exchange reaction channel is not observed at room temperature, its branching ratio increases up to 21% at high energies (although neither the contribution of each excited N atom nor the kinetic energy was originally shown),[78,79] which can be compared with the QCT value of 3.02% at 1500 K (Table VIII). Nonetheless, lower QCT branching ratios for this reaction would be obtained by using the total $N(^2D)+NO$ rate constant.

C. Dynamical properties

As refers to the mode of reaction, the existence of several reaction pathways through which the system can evolve along the $^1A'$ PES has been discussed in Sec. III in terms of

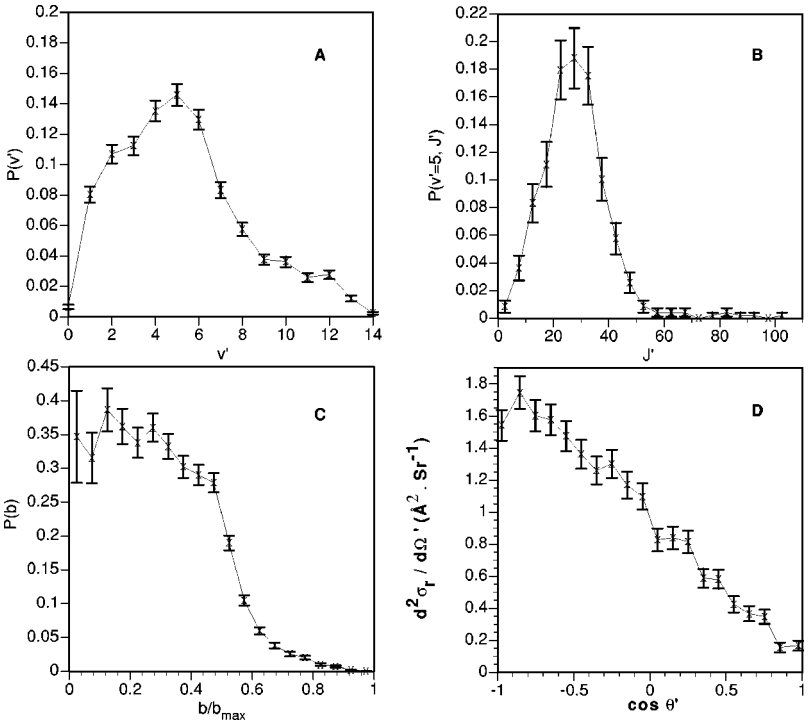

FIG. 6. QCT properties of reaction (8) at $T=300$ K: (a) N_2 vibrational distribution; (b) N_2 rovibrational distribution at $v'=5$; (c) opacity function and (d) differential reaction cross-section for the scattering angle θ'. Error bars show one standard deviation.

the labeled routes 1, 2 and 3. The existence of a deep potential well (i.e., the stable NNO molecule) could have a strong effect on the dynamics by means of the formation of short-or long-lived collision complexes. It is known that such collision complexes can facilitate the intramolecular energy redistribution and affect the product properties [e.g., the rovibrational distributions and differential cross-sections (DCS)]. On the other hand, though the magnitude of the entrance barriers facilitates an attack of the $N(^2D)$ atom to the nitrogen side of its counterpart NO molecule, traversing TS 1 and heading for the NNO minimum, in some trajectories the $N(^2D)$ atom could attach to the NO oxygen side, overcoming the TS 4 barrier. Moreover, passage through TS 9, which links both routes of reaction, is also possible.

As an aid to classify the different types of trajectories, an estimation of the lifetimes τ of the collision complexes (i.e., an estimation of the time the nuclei spent in close proximity), combined with visual inspection (i.e., geometry and potential energy evolutions) of samples of reactive trajectories was carried out. The analysis for reaction at 300 K indicates that most of the trajectories (about 95%) pass only through the NNO minimum spending much less than 0.1 ps (i.e., direct trajectories) and producing directly products through route 1. Only about 1% of the trajectories presents longer lifetimes for this route. The rest of trajectories show lifetimes between 0.1 and 1.2 ps, evolving through route 2 (about 0.5%) and route 3 (about 3.5%). At higher temperatures there is a significant augment of the routes 2 and 3 (see Table VIII).

Several QCT-derived reaction properties in products have also been analyzed and summarized in Table VIII. The mean fraction of the total energy which channels into each mode of motion in products, i.e., translational (T'), vibrational (V') and rotational (R'), was computed performing an average of the ratio E_I'/E_{tot} over all reactive trajectories, where I' stands for a particular mode of motion. The resulting fractions show the tendency of reaction (8) to produce a similar percentage of energy channeled into translation and vibration (although $\langle f_T' \rangle \geqslant \langle f_V' \rangle$), and a low percentage into rotation, which can be understood considering the evolution of the most of the trajectories (i.e., route 1), which form collision complexes close to colinear NNO structures. At higher temperatures the trajectories can evolve through less attractive regions of the PES (i.e., bent NNO structures) and the rotational excitation can increase. The comparison of these energy fractions with the QCT values obtained for the similar barrierless $N(^4S)+NO$ reaction (i.e., $\langle f_T' \rangle = 0.63$, $\langle f_V' \rangle = 0.28$ and $\langle f_R' \rangle = 0.09$ at 300 K[80]) shows a reasonable behavior, as for this latter reaction (with analogous kinematics, H+HH, H=heavy) the preferred bent geometries and the absence of a minimum produce less vibrational and more rotational excitation. In both reactions, the increase in temperature (or E_T) produces mainly almost constant $\langle f_V' \rangle$ fractions, an increase in $\langle f_R' \rangle$ and the corresponding reduction in $\langle f_T' \rangle$.

QCT vibrational distributions are inverted and peak at $v'=5$ at 300 K [Fig. 6(a)] and at higher v' values for larger temperatures (e.g., $v'=9$ at 1000 K), as expected for a reaction with a high exothermicity. All the thermodynamically accessible vibrational levels are populated. The shoulder observed in the distribution [Fig. 6(a)] at the highest values of v' does not seem to correspond to a particular mode of reaction. Although the more complex trajectories tend to give a vibrational distribution where these larger values of v' are more populated than for the average of all the reactive trajectories, they do not account for all the observed increment in this zone. Besides, it must be noted that the number of such trajectories was not sufficient to allow for a reliable statistics. The rotational distribution for the $v'=5$ maximum is shown in Fig. 6(b). It presents a maximum at about J'

=25, which would correspond to a Maxwell–Boltzmann distribution with a temperature of around 3500 K. Again, the more complex trajectories yield values of J' somewhat higher than those corresponding to a distribution peaking at $J'=25$. Both the vibrational and rotational distributions have been normalized to unit area such that they actually represent a probability.

The opacity function and the DCS for the scattering angle θ' (forward for $\theta'<90°$ and backward for $\theta'>90°$) are presented in Figs. 6(c) and 6(d), respectively, for $T=300\,\mathrm{K}$. In the former it is patent that most trajectories present low impact parameters, less or equal to half the maximum value of 6.0 Å. This would be in accordance with a dominant head-on attack which requires low impact parameters. This main mechanism along with the rather direct character of most trajectories is in accordance with the predominant backward scattering (i.e., rebound mechanism) with few forward trajectories in the DCS representation. The mean value of the scattering angle calculated over all trajectories is around 110° (i.e., shifted to backward angles). In particular, the trajectories exploring only the NNO minimum are slightly shifted towards backward angles, whereas those reaching the NON structures are more evenly distributed over all scattering angles. However, we recall that the small number of complex trajectories does not allow one to come to conclusions of statistical significance. On the other hand, the trajectories following route 1 have mainly very short collision times ($\tau \leqslant 0.01\,\mathrm{ps}$), of the same order as the vibrational periods τ_{vib} (i.e., 0.015, 0.027 and 0.18 ps for the NNO minimum) but much shorter than the lowest estimated rotational periods τ_{rot} (i.e., 1.2 ps at 300 K or 0.62 ps at 1500 K calculated as $2\pi I/\langle L\rangle$ with the NNO principal inertia moments and an average total angular momentum over the reactive trajectories). Hence, most of collision complexes in route 1 will last only during one vibration but without almost time for a rotation, which will not produce symmetrical DCSs as QCT result display. At higher temperatures it is observed an increase of the forward/backward ratio but both τ and τ_{rot} decrease (i.e., $\tau_{\mathrm{rot}}=0.62\,\mathrm{ps}$ at 1500 K). Hence, the symmetrical (almost flat) DCS at 1500 K can be rationalized in terms of the enhancement of the stripping mechanism with mainly forward scattering, usually observed when collision energies are increased in similar reactions.[80]

A more extensive study with larger batches of reactive trajectories and with different detailed reactants conditions (i.e., E_T,v,J) is in progress to provide further insight on the different mechanisms and their extent for this rather complicated reaction with two parallel reaction channels.

V. CONCLUSIONS AND REMARKS

In this work we present an extensive theoretical study of the $\mathrm{N}(^2D)+\mathrm{NO}(X\,^2\Pi)\rightarrow\mathrm{O}(^1D)+\mathrm{N}_2(X\,^1\Sigma_g^+)$ exothermic reaction on its lowest $^1A'$ potential energy surface. *Ab initio* CASSCF(16,12) and CASPT2(16,12) methods with the standard Cartesian 6-311G(2d) basis set have been used to characterize all stationary points. Thus, several minima and transition states have been found along the different MEPs connecting reactants and products, although a barrierless reaction is predicted on this lowest PES. Apart from the NNO molecule, two relatively stable NNO isomers, a linear $\mathrm{NON}(^1\Sigma_g^+)$ minimum and a cyclic-$C_{2v}(^1A_1)$ minimum, have been also located. The results are in good agreement with previous high quality *ab initio* studies and with some assumptions made in experimental works, and the energy ordering found is $\mathrm{NNO}(^1\Sigma^+)<\text{cyclic-}C_{2v}\mathrm{NON}(^1A_1)<\mathrm{NON}(^1\Sigma_g^+)$.

The excellent results obtained for reactants and products of this reaction (8) as well as for the N_2O isomers and the $(1\,^1A',2\,^1A')$ surface crossing in comparison with preceding *ab initio* data and with available experimental data, point towards the suitability of describing the ground $^1A'$ NNO PES at the CASPT2(16,12)/6-311G(2d) level of theory. Thus, an analytical PES has been constructed by fitting a grid of approximately 1250 points. The goodness of the fit is validated by the small RMSD (i.e., 1.12 kcal/mol) and by the accurate fitting of all *ab initio* stationary points.

A QCT study of this reaction at several temperatures (300–1500 K) was also carried out. Reaction cross-sections, thermal rate constants and energy and angular product distributions were determined. A comparison of the QCT rate constant (i.e., k_8) with the experimental total removal rate of $\mathrm{N}(^2D)$ by NO at 300 K (i.e., k), indicates that the inclusion of the excited PESs in reaction (8) does not account for the experimental k value; possibly, it should also be necessary the addition of the two rate constants of the parallel $\mathrm{N}(^2D)+\mathrm{NO}(X\,^2\Pi)\rightarrow\mathrm{O}(^1S,\,^3P)+\mathrm{N}_2(X\,^1\Sigma_g^+)$ (7,9) reactions. Our preliminary *ab initio* study of the $^3A''$ PES involved in reaction (9) reports a barrierless MEP and therefore stresses the importance of this parallel reaction. Further calculations are in progress to determine a precise k_9 value. Moreover, it is also concluded that the physical electronic quenching process (10) should be unimportant in these conditions. On the other hand, at higher temperatures the N-exchange reaction (6) becomes more important (i.e., 3.02% of the branching ratio at 1500 K) in accord with experimental data; the total rate constant would also increase a bit more with this apportionment.

The dynamics of this reaction at 300 K presents a predominant reaction pathway (i.e., 96%) with very short-lived collision complexes around the NNO minimum. This microscopic mechanism with rather direct trajectories produces a similar percentage of energy channeled into vibration (although with an inverted distribution at $v'=5$) and translation, and a low percentage into rotation, with fundamentally backward scattering (i.e., rebound mechanism). At higher temperatures the shift in the reaction attributes shows the expected behavior; also, the reaction pathways involving NON structures become increasingly important and a larger statistics (now in progress) should be necessary in order to analyze in more detail the dynamics in these other energy conditions.

ACKNOWLEDGMENTS

This work has been supported by the ''Dirección General de Enseñanza Superior (Programa Sectorial de Promoción General del Conocimiento)'' of the Spanish Ministry of

Education and Culture (DGES Project Ref. PB 98-1209-C02-01). Financial support from the European Union (INTAS Project Ref. 99-00701) and the ''Generalitat'' (Regional Government) of Catalonia (Project Ref. 1998SGR 0008) is also acknowledged. R. V. also thanks the ''Generalitat'' for a ''beca de formació d'investigadors'' research grant. The authors are also grateful to the ''Center de Computació i Comunicacions de Catalunya (CESCA/CEPBA)'' for providing a part of the computer time.

[1] P. Warneck, in *Chemistry of the Natural Atmosphere* (Academic, San Diego, 1998), Chap. 3.
[2] M. W. Chase, Jr., C. A. Davies, J. R. Downey, Jr., D. J. Frurip, R. A. McDonald, and A. N. Syverud, J. Phys. Chem. Ref. Data **14** (1985), Suppl. 1.
[3] M. Brouard, S. P. Duxon, P. A. Enriquez, R. Sayós, and J. P. Simons, J. Phys. Chem. **95**, 8169 (1991).
[4] A. J. Alexander, F. J. Aoiz, M. Brouard, I. Burak, Y. Fujimura, J. Short, and J. P. Simons, Chem. Phys. Lett. **262**, 589 (1996).
[5] Y. Hsu, J. Wang, and K. Liu, J. Chem. Phys. **107**, 2351 (1997).
[6] H. Tachikawa, K. Ohnishi, T. Hamabayashi, and H. Yoshida, J. Phys. Chem. A **101**, 2229 (1997).
[7] E. R. Fisher and E. Bauer, J. Chem. Phys. **57**, 1966 (1972).
[8] Y. Matsumi and A. M. S. Chowdhury, J. Chem. Phys. **104**, 7036 (1996).
[9] G. E. Streit, C. J. Howard, A. L. Schmeltekopf, J. A. Davidson, and H. I. Schiff, J. Chem. Phys. **65**, 4761 (1976).
[10] D. Bose and G. V. Candler, J. Chem. Phys. **104**, 2825 (1996), and references therein.
[11] A. Aguilar, M. Gilibert, X. Giménez, M. González, and R. Sayós, J. Chem. Phys. **103**, 1 (1995) and references therein.
[12] K. Sugawara, Y. Ishikawa, and S. Sato, Bull. Chem. Soc. Jpn. **53**, 3159 (1980).
[13] H. Umemoto, N. Hachiya, E. Matsunaga, A. Suda, and M. Kawasaki, Chem. Phys. Lett. **296**, 203 (1998).
[14] D. G. Hopper, J. Chem. Phys. **80**, 4290 (1984).
[15] R. J. Donovan and D. Husain, Chem. Rev. **70**, 489 (1970).
[16] G. Herzberg and L. Herzberg, J. Chem. Phys. **18**, 1551 (1950).
[17] C. Amiot and G. Guelachvili, J. Math. Phys. **51**, 475 (1974).
[18] C. Amiot and G. Guelachvili, J. Mol. Spectrosc. **59**, 171 (1976).
[19] A. Campargue, D. Permogorov, M. Bach, M. A. Temsamani, J. V. Auwera, M. Herman, and M. Fujii, J. Chem. Phys. **103**, 5931 (1995).
[20] C. Amiot, J. Mol. Spectrosc. **59**, 191 (1976).
[21] M. D. Vanek, M. Schneider, J. S. Wells, and A. G. Maki, J. Mol. Spectrosc. **134**, 154 (1989).
[22] R. A. Toth, Appl. Opt. **30**, 5289 (1991).
[23] I. Suzuki, J. Mol. Spectrosc. **32**, 54 (1969).
[24] A. Chédin, C. Amiot, and Z. Cihla, J. Mol. Spectrosc. **63**, 348 (1976).
[25] M. Lacy and D. H. Whiffen, Mol. Phys. **45**, 241 (1982).
[26] M. Kobayashi and I. Suzuki, J. Mol. Spectrosc. **125**, 24 (1987).
[27] J. L. Teffo and A. Chédin, J. Mol. Spectrosc. **135**, 389 (1989).
[28] J. L. Teffo, V. I. Perevalov, and O. M. Lyulin, J. Mol. Spectrosc. **168**, 390 (1994).
[29] W. D. Allen, Y. Yamaguchi, A. G. Császár, D. A. Clabo, Jr., R. B. Remington, and H. F. Schaeffer III, Chem. Phys. **145**, 427 (1990).
[30] J. M. L. Martin, P. R. Taylor, and T. J. Lee, Chem. Phys. Lett. **205**, 535 (1993).
[31] W. D. Allen and A. G. Császár, J. Phys. Chem. **98**, 8823 (1994).
[32] A. G. Császár, J. Phys. Chem. **98**, 8823 (1994).
[33] A. T. Wong and G. B. Backsay, Chem. Phys. Lett. **207**, 360 (1993).
[34] S. D. Peyerimhoff and R. J. Buenker, J. Chem. Phys. **49**, 2473 (1968).
[35] P. Pyykkö, Chem. Phys. Lett. **156**, 337 (1989).
[36] M. J. Crawford and T. M. Klapötke, Inorg. Chem. **38**, 3006 (1999).
[37] F. Wang and R. D. Harcourt, J. Phys. Chem. A **104**, 1304 (2000).
[38] M. A. Vincent, I. H. Hillier, and L. Salsi, Phys. Chem. Chem. Phys. **2**, 707 (2000).
[39] I. C. Tornieporth-Oetting and T. M. Klapötke, Angew. Chem. Int. Ed. Engl. **34**, 511 (1995).
[40] J. M. Galbraith and H. F. Schaeffer III, J. Am. Chem. Soc. **118**, 4860 (1996).
[41] H. Nakamura and S. Kato, J. Chem. Phys. **110**, 9937 (1999).
[42] A. Brown, P. Jimeno, and G. G. Balint-Kurti, J. Phys. Chem. A **103**, 11089 (1999).
[43] J. M. Teule, G. C. Groenenboom, D. W. Neyer, D. W. Chandler, and M. H. M. Janssen, Chem. Phys. Lett. **320**, 177 (2000).
[44] GAUSSIAN98, Revision A.7, M. J. Frisch, G. W. Trucks, H. B. Schlegel *et al.*, Gaussian, Inc., Pittsburgh, PA, 1998.
[45] MOLCAS 4.1, K. Andersson, M. R. A. Blomberg, M. P. Fülscher *et al.*, Lund University, Sweden, 1998.
[46] B. O. Roos, P. R. Taylor, and P. E. M. Siegbahn, Chem. Phys. **48**, 157 (1980).
[47] B. O. Roos, in *Advances in Chemical Physics: Ab Initio Methods in Quantum Chemistry—II*, edited by K. P. Lawley (Wiley, Chichester, 1987), Vol. LXIX, p. 399.
[48] K. Andersson, Theor. Chim. Acta **91**, 31 (1995).
[49] R. Krishnan, J. S. Binkley, R. Seeger, and J. A. Pople, J. Chem. Phys. **72**, 650 (1980).
[50] M. J. Frisch, J. A. Pople, and J. S. Binkley, J. Chem. Phys. **80**, 3265 (1984).
[51] Extensible Computational Chemistry Environment Basis Set Database, Version 1.0, as developed and distributed by the Molecular Science Computing Facility, Environmental and Molecular Sciences Laboratory (EMSL) which is a part of the Pacific Northwest Laboratory, P.O. Box 999, Richland, Washington 99352, USA, and funded by the U.S. Department of Energy.
[52] R. Sayós, R. Valero, J. M. Anglada, and M. González, J. Chem. Phys. **112**, 6608 (2000).
[53] K. P. Huber and G. Herzberg, in *Molecular Spectra and Molecular Structure. Vol. IV. Constants of Diatomic Molecules* (Van Nostrand Reinhold, New York, 1979).
[54] S. Bashkin and J. O. Stoner, Jr., in *Atomic Energy Levels and Grotrian Diagrams* (North-Holland, Amsterdam, 1975), Vol. I.
[55] SURVIBTM, W. C. Ermler, H. C. Hsieh, and L. B. Harding, Comput. Phys. Commun. **51**, 257 (1988).
[56] G. Simons, R. G. Parr, and J. M. Finlan, J. Chem. Phys. **59**, 3229 (1973).
[57] G. Simons, J. Chem. Phys. **61**, 369 (1974).
[58] H. Okabe, in *Photochemistry of Small Molecules* (Wiley, New York, 1978).
[59] J. L. Whitten, J. Chem. Phys. **44**, 359 (1966).
[60] M. A. Bearpark, M. A. Robb, and H. B. Schlegel, Chem. Phys. Lett. **223**, 269 (1994).
[61] A. H. H. Chang and D. R. Yarkony, J. Chem. Phys. **99**, 6824 (1993).
[62] H. C. Longuet-Higgins, Proc. R. Soc. London, Ser. A **344**, 147 (1975).
[63] G. J. Atchity, S. S. Xantheas, and K. Ruedenberg, J. Chem. Phys. **95**, 1862 (1991).
[64] J. N. Murrell, S. Carter, S. C. Farantos, P. Huxley, and A. J. C. Varandas, in *Molecular Potential Energy Surfaces* (Wiley, New York, 1984).
[65] DIATOMFIT, M. González and R. Sayós (unpublished program).
[66] SM3FIT, R. Sayós and M. González (unpublished program).
[67] TRIATOM, J. Tennyson, S. Miller, and C. R. Le Sueur, Comput. Phys. Commun. **75**, 339 (1993).
[68] TRIQCT, R. Sayós and M. González (unpublished program).
[69] D. G. Truhlar, and J. T. Muckerman, in *Atom–Molecule Collision Theory. A Guide for the Experimentalist*, edited by R. B. Bernstein (Plenum, New York, 1979), Chap. 16.
[70] N. C. Blais and D. G. Truhlar, J. Chem. Phys. **65**, 5335 (1976).
[71] W. B. DeMore, D. M. Golden, R. F. Hampson, M. J. Kurylo, C. J. Howard, A. R. Ravishankara, C. E. Kolb, and M. J. Molina, in *Chemical Kinetics and Photochemical Data for Use in Stratospheric Modelling*, in Evaluation 12, JPL Publ. 97-4 (Jet Propulsion Laboratory, Pasadena, CA, 1997).
[72] S. P. Walch and R. L. Jaffe, J. Chem. Phys. **86**, 6946 (1987).
[73] T. Suzuki, Y. Shihira, T. Sato, H. Umemoto, and S. Tsunashima, J. Chem. Soc., Faraday Trans. **89**, 995 (1993).
[74] M. González, I. Miquel, and R. Sayós, manuscript in preparation.
[75] Y. Kurosaki and T. Takayanagi, J. Phys. Chem. A **103**, 436 (1999).
[76] Y. Kurosaki, T. Takayanagi, K. Sato, K. Misawa, Y. Mobayashi, and S. Tsunashima, J. Phys. Chem. A **103**, 250 (1999).
[77] T. Takayanagi, Y. Kurosaki, K. Sato, and S. Tsunashima, J. Phys. Chem. A **102**, 10391 (1998).
[78] J. Dubrin, C. MacKay, and R. Wolfgang, J. Chem. Phys. **44**, 2208 (1966).
[79] R. Iwata, R. A. Ferrieri, and A. Wolf, J. Phys. Chem. **90**, 6723 (1986).
[80] M. Gilibert, A. Aguilar, M. González, F. Mota, and R. Sayós, J. Chem. Phys. **97**, 5542 (1992).